



Simulating surface and subsurface initiation of macropore flow

Markus Weiler^{a,*}, Felix Naef^{b,1}

^aDepartment of Forest Engineering, Oregon State University, Corvallis, OR 97331-570 6, USA

^bInstitute of Hydromechanics and Water Resources Management, HIF C 44, Swiss Federal Institute of Technology Zürich, CH-8093 Zürich, Switzerland

Received 25 January 2002; revised 7 November 2002; accepted 8 November 2002

Abstract

Initiation of macropore flow either from the soil surface or from a saturated soil layer at depth is a first order control on water flow in macropores and water transfer from macropores into the surrounding soil matrix. Nevertheless, these initiation processes have not been well documented. We surveyed surface topography at four field sites with permanent grass vegetation with grid spacing of 10 cm and applied Kriging to derive the spatial correlation structure. We then simulated the water flux into macropores based on different combinations of surveyed surface micro-topographies, spatial earthworm burrow distributions, and the soil properties, to examine more fully the role of macropore drainage area (MDA) on macropore flow initiation. The spatial distributions of the earthworm burrows were derived from horizontal soil sections extracted from each study profile. The MDA was calculated for different sets of surface topography and macropore density using a flow accumulation algorithm. The resulting MDA of each macropore was used to calculate the total relative MDA, which is equal to the proportion of overland flow draining into macropores, and the MDA probability distribution. The results showed that the macropore density primarily controlled the total MDA and that surface micro-topography strongly influenced the probability distribution of the MDA. Only a few macropores contributed significantly to the total macropore flow whereas the majority of macropores received little water; a phenomenon especially pronounced for a rough surface topography and for a low soil surface gradient. The simulated probability distribution of subsurface initiation was very different from the distribution derived for surface initiation; more symmetrical, less variable and slightly influenced by the roughness and the gradient of the interface between the saturated and the low permeable soil layer. We conclude that the different amount of water supplied to each macropore further alters the percolation depth and transport of solutes in macroporous soils and should be considered for modelling infiltration in macroporous soils.

© 2003 Published by Elsevier Science B.V.

Keywords: Macropore flow; Micro-topography; Preferential flow; Earthworm burrows; Infiltration

1. Introduction

Macropores influence the infiltration of rainfall and therefore runoff and solute transport in natural soils, in which these structures are common (Larson, 1999). Infiltrating water flows rapidly in structural pore spaces such as worm channels, shrinking cracks, and

* Corresponding author. Tel.: +1-541-737-8719; fax: +1-541-737-4316.

E-mail addresses: markus@2hydros.de (M. Weiler), naef@ihw.baug.ethz.ch (F. Naef).

¹ Tel.: +41-1-633-3384; fax: +41-1-633-1224.

97 root holes and can subsequently bypass portions of the
 98 soil profile. The impact of macropores is governed
 99 primarily by the water supply to macropores, the
 100 water flow in macropores, and the water transfer from
 101 the macropores into the surrounding soil matrix
 102 (Beven and Germann, 1982; Faeh et al., 1997; Buttle
 103 and House, 1997). The causes and extent of
 104 preferential flow and particularly macropore flow,
 105 which is a subset of preferential flow, are poorly
 106 known (Flühler et al., 1996). In particular, the controls
 107 on vertical macropore flow by surface and subsurface
 108 initiation should be further examined.

109 This study concentrates on macropore systems
 110 caused by earthworm activity, a prime macropore
 111 generating factor in natural soils in many climatic
 112 regions. Especially the anecic earthworm species
 113 *Lumbricus terrestris* generates vertically oriented,
 114 highly continuous channels (e.g. Langmaack et al.,
 115 1999). Different experimental studies have shown that
 116 the maximum flow rate in macropores that are built by
 117 anecic earthworm species lies within a narrow range
 118 of $1\text{--}7\text{ cm}^3\text{ s}^{-1}$ (Bouma et al., 1982; Wang et al.,
 119 1994; Shipitalo and Gibbs, 2000). The surveyed
 120 macropore density varies between 45 and 700 m^{-2}
 121 depending on vegetation, climate, soil management,
 122 etc. (Ehlers, 1975; Trojan and Linden, 1998;
 123 Munyankusi et al., 1994; Zehe and Flühler, 2001). If
 124 we assume a low macropore density of 100 m^{-2} , the
 125 total possible flow rate of the macropore system
 126 ranges from 360 to 2520 mm h^{-1} . These rates are
 127 many times that of naturally occurring rainfall
 128 intensities. Thus, the flow rate of the macropore
 129 system itself is usually not a limiting factor during the
 130 infiltration process, and may in fact be a process
 131 enhancing infiltration (Weiler, 2001).

132 Macropore flow initiation during infiltration is a
 133 function of initial matrix water content, rainfall
 134 intensity, rainfall amount, matrix hydraulic conduc-
 135 tivity, and soil surface contributing area (Trojan and
 136 Linden, 1992). Water can flow into macropores either
 137 from the soil surface or from a saturated or partially
 138 saturated soil layer at depth. Subsurface initiation of
 139 macropore flow occurs only if specific arrangements
 140 and properties of the soil exist that allow for
 141 interaction between matrix water and the macropore
 142 void space (Ela et al., 1992; Li and Ghodrati, 1997;
 143 Weiler et al., 1998). Whilst some studies have shown
 144 that macropore density, slope, and roughness of

the surface influence the surface initiation (Trojan 145
 and Linden, 1992; Léonard et al., 1999), the controls 146
 on macropore flow initiation, infiltration and solute 147
 transport are still not well understood. 148

149 Few studies have directly observed or quantified
 150 macropore initiation. Laboratory experiments cannot
 151 reproduce the complex natural relations between the
 152 soil surface, the vegetation, and the macropores.
 153 Artificial macropores are often only useful to study a
 154 selected detail of the initiation process (e.g. Phillips
 155 et al., 1989). However, some laboratory experiments
 156 with grid lysimeters, which measure the outflow
 157 variability below a soil block in a grid collector
 158 system, have shown that flow in macropores can be
 159 highly variable, probably due to a variable initiation
 160 of macropore flow (Andreini and Steenhuis, 1990;
 161 Shipitalo et al., 1990; Edwards et al., 1992; Bowman
 162 et al., 1994; Quisenberry et al., 1994). Field
 163 measurements to directly observe surface initiation
 164 are difficult or even impossible because vegetation
 165 often covers the surface and thus prevents visual
 166 observation and recording. Removing the vegetation
 167 cover alters the surface characteristics and the
 168 infiltration controls that one seeks to measure. Indirect
 169 measurements of the soil water content and the matric
 170 potential in combination with dye experiments may
 171 only verify whether macropore initiation has taken
 172 place at the soil surface or within the soil (Weiler and
 173 Naef, 2002).

174 This paper describes a new approach to measure
 175 and simulate the initiation of water flux into macro-
 176 pores from both the soil surface and subsurface layers.
 177 We surveyed the surface topography and the earth-
 178 worm generated macropore distributions on four field
 179 sites and used these data to calculate the surface area
 180 draining into each macropore. The resulting flow rate
 181 distributions in the macropores are then assessed and
 182 the main controls of the initiation process are
 183 systematically analysed for surface and subsurface
 184 initiation. Specifically our objectives were: 184

- 185 1. How does the macropore density influence the total 186
 MDA and thus the infiltration behaviour of soils for 187
 surface initiation? 188
- 189 2. How do the macropore density, the hillslope 190
 gradient, and the surface roughness influence the 191
 MDA probability distribution and thus the flow rate 192
 distribution in the macropores for surface initiation? 192

- 193 3. How do macropore density, spatial variable satu- 241
 194 rated hydraulic conductivity, and spatial variable 242
 195 soil horizon boundaries influence the initiation 243
 196 probability distribution under non-steady state 244
 197 conditions for subsurface initiation and how does 245
 198 the non-steady state simulations compare to the 246
 199 steady state solution? 247
 200 4. How compares the resulting macropore flow rate 248
 201 distribution of surface initiation to subsurface 249
 202 initiation? 250

203
 204 Finally, simulation results are compared with 251
 205 findings from sprinkling and dye tracer experiments 252
 206 (Weiler and Naef, 2002) and various other published 253
 207 laboratory experiments. Implications on water and 254
 208 solute transport in soils with macropores are 255
 209 discussed. 256

210 2. Methods 257

211 2.1. Field sites 258

212
 213
 214 The soil surface topography and the macropore 259
 215 distribution data were collected from four field sites in 260
 216 Switzerland. On these sites the processes and 261
 217 regulation mechanisms of macropore flow with 262
 218 respect to infiltration have been extensively studied 263
 219 with combined sprinkling and dye tracer experiments 264
 220 with different rainfall intensities and initial soil 265
 221 moisture conditions (Weiler, 2001; Weiler and Naef, 266
 222 2002). All sites have been covered by grassland for at 267
 223 least 20 years. Thus, they provide an undisturbed 268
 224 record of the macropore network development by 269
 225 earthworm activity in the soil (Syers and Springett, 270
 226 1983). Table 1 summarizes the sites' soil properties, 271
 227 soil classification, geological parent material, and soil 272
 228 properties of individual soil horizons. 273

229 2.2. Surface topography characterization 274

230
 231 A detailed examination of the micro-topography 275
 232 of the soil surface is a prerequisite for simulating 276
 233 macropore flow initiation at the soil surface. We 277
 234 manually surveyed the soil surface topography for an 278
 235 area of 290 cm by 100 cm at each of the four sites 279
 236 using a grid spacing of 10 cm. Table 2 summarizes 280
 237 the average slope and the 'deviation of the surface 281
 238

241 from a fitted plane' at each site. Kriging was then 242
 243 applied to increase the spatial resolution of the 244
 245 measured soil surface data. Kriging conserves the 246
 247 spatial correlation of the topography and can 248
 249 incorporate possible anisotropy and underlying 250
 251 trends not apparent in the raw gridded data 252
 252 (Huang, 1998). Because the surface topography 253
 254 was accurately measured, an exact interpolation 254
 255 method like Kriging without nugget effect was 255
 256 used. An experimental variogram was calculated 256
 257 for the four sites, after a plane was fitted to the 257
 258 measured values and subtracted from the values to 258
 259 incorporate the drift of the data (Stein, 1999). 259
 260 Anisotropy was not detected. All experimental 260
 261 variograms showed an exponential behaviour and 261
 262 no nugget effect. Therefore, an exponential model 262
 263 with an anisotropy ratio of one was fitted to the 263
 264 experimental semi-variogram: 264

$$265 \gamma(h) = C \left[1 - \exp\left(-\frac{h}{a}\right) \right] \quad (1) \quad 266$$

267 where $\gamma(h)$ is the semi-variogram, C is the scale or 267
 268 sill for the structured component of the variogram, a 268
 269 is the range, and h is the separation distance. The 269
 270 derived parameters of the exponential model for the 270
 271 sites are listed in the last two columns of Table 2. 271

272 2.3. Spatial macropore distribution 272

273 If the stochastic process generating the spatial 273
 274 pattern of macropores is known, initiation can be 274
 275 simulated for different realisations of macropore 275
 276 distributions. The spatial distribution of the macro- 276
 277 pores at the soil surface and the macropore density 277
 278 were surveyed at each site across four horizontal soil 278
 279 sections 1–2 cm below the surface (details on the 279
 280 preparation of the sections in Weiler, 2001). Photos of 280
 281 the 100 cm by 50 cm sections were taken and 281
 282 macropores larger than 1 mm² were classified using 282
 283 image analysis (Weiler, 2001). The spatial pattern of 283
 284 macropores and the related distribution of distances 284
 285 from a point to the nearest macropore are important 285
 286 properties influencing initiation and macropore- 286
 287 enhanced infiltration (Droogers et al., 1998). The 287
 288 nature of the processes generating a point pattern can 288
 289 be evaluated with quadrature analysis (Smettem and 289
 290 Collis-George, 1985; Brimicombe and Tsui, 2000). 290
 291 The Index of Cluster Size (ICS), which can be 291

289 Table 1
290 Soil properties of the experimental sites

291 Site	292 Soil classification ^a	293 Geological parent material	294 Average values for distinct soil horizons				
			295 Depth (cm)	296 Density (g cm ⁻³)	297 Soil texture ^b	298 K_{sat} ^c (mm h ⁻¹)	299 n_{mac} ^d (mm ⁻²)
300 Rietholz-bach	301 Mollic Cambisol	302 Conglo-merates (molasse)	303 0–30	304 1.14	305 Loam	306 12.0	307 95
			308 30–60	309 1.25	310 Loam	311 9.6	312 155
			313 60–100	314 1.35	315 Clay loam	316 4.7	317 90
			318 0–20	319 1.34	320 Loam	321 6.5	322 210
323 Heiters-berg	324 Umbric Cambisol	325 Moraine	326 20–45	327 1.57	328 Loam	329 1.9	330 140
			331 45–100	332 1.66	333 Loam	334 1.4	335 93
			336 0–15	337 1.31	338 Silt loam	339 10.7	340 154
341 Koblenz	342 Eutric Cambisol	343 Moraine	344 15–45	345 1.35	346 Silt loam	347 3.8	348 196
			349 45–90	350 1.51	351 Loam	352 2.1	353 88
			354 0–30	355 1.41	356 Sandy clay loam	357 15.4	358 186
360 Nieder-weningen	361 Eutric Cambisol	362 Sandstone (molasse)	363 30–55	364 1.44	365 Sandy loam	366 29.3	367 322
			368 55–100	369 1.42	370 sandy loam	371 54.8	372 185

373 ^a Food and Agricultural Organization (1974)

374 ^b Soil Survey Staff (1951)

375 ^c Saturated hydraulic conductivity of the soil matrix determined from soil texture and bulk density (Schaap and Leij, 2000)

376 ^d Macropore density was determined from macropore with an area larger than 1 mm² and a circular shape using image analysis of the horizontal soil sections (Weiler, 2001)

377 calculated from the point counts in each quadrat, is
378 a straightforward method to account for this gener-
379 ation process:

$$380 \text{ICS} = \frac{s^2}{\bar{x}} - 1 \quad (2)$$

381 where \bar{x} is the mean and s^2 is the variance of the
382 counts in each quadrat. An $\text{ICS} > 0$ shows the
383 existence of clustered pattern, $\text{ICS} < 0$ implies a
384 uniform pattern, and $\text{ICS} = 0$ indicates a random
385 pattern. The ICS depends on the quadrat size (if the
386 data set is not synthetic) because the generation
387 process of non-synthetic data is usually scale
388 dependent.

377 In this study, macropores classified from the
378 horizontal sections were used to calculate the ICS.
379 Verification of the image analysis procedure resulted
380 in correct classification of 90% of the macropores
381 (Weiler, 2001). To account for scale effects, the size
382 of the quadrats were varied calculating the ICS. The
383 centre of each classified macropore was determined
384 and the resulting point pattern was used to derive the
385 ICS. Table 3 shows the average ICS for each site of
386 the four horizontal sections. The values show that the
387 underlying generation process of the macropore
388 pattern is random except for large quadrats where
389 the point pattern tends to be more clustered. The
390 higher values for large quadrat sizes at the Koblenz

391 Table 2
392 Characterisation of the surface topography of the four experimental sites

393 Site	394 Slope (%)	395 Absolute deviation of the surface (mm)				396 Variogram	
		397 Average	398 Median	399 25% quantile	400 75% quantile	401 a (cm)	402 C
403 Rietholz-bach	404 22.1	405 7.8	406 6.0	407 3.0	408 10.9	409 43.8	410 1.35
411 Heitersberg	412 22.9	413 6.6	414 5.5	415 2.5	416 9.1	417 93.1	418 1.90
419 Koblenz	420 16.4	421 14.6	422 10.1	423 4.4	424 18.1	425 42.5	426 1.34
427 Niederweningen	428 16.2	429 14.0	430 8.0	431 3.6	432 14.4	433 26.8	434 1.16

Table 3
Average Index of Cluster Size (ICS) for each site with a variable quadrat size

Site	Index of Cluster Size (ICS) for quadrat size			
	5 cm	10 cm	30 cm	50 cm
Rietholzbach	0.003	0.025	0.053	0.073
Heitersberg	−0.004	0.005	0.084	0.144
Koblenz	−0.006	0.020	0.262	0.558
Niederweningen	0.000	0.037	0.385	0.719

and Niederweningen sites (Table 3) are influenced by ant activity and mouse holes. Notwithstanding, the pattern of the macropores formed by earthworm activity is a random point pattern. Smettem and Collis-George (1985) also showed that spatial patterns of earthworm channels are random for grassland soils. The Poisson process is the simplest possible stochastic mechanism to generate the random spatial distribution of this type of macropore (Diggle, 1983).

2.4. Modelling of surface initiation

With knowledge of the site surface topography, the macropore density, and the spatial pattern of the macropores near the soil surface, a description and simulation of the soil surface macropore initiation was sought. If one assumes steady state conditions, uniform rainfall distribution, a homogeneous hydraulic conductivity of the soil matrix around the macropores, and that the surface topography is not affected by the rain itself, then the rainfall not infiltrating into the soil matrix flows according to the soil topography. If the water flows into a macropore open at the surface, it will completely ‘disappear’ since the vertical flow rate in a single earthworm channel is large relative to the surface flow (Weiler, 2001). Consequently, the area that drains to a macropore (i.e. the local upslope contributing area of the vertical hole opening) determines the amount of water flowing in the macropore. Thus, the inflow quantity of each macropore is proportional to its macropore drainage area (MDA). The inflow q (mm h^{-1}) into a macropore i is then given as:

$$q_i = (p - i_{\text{mat}}) \text{MDA}_i n_{\text{mac}} \quad (3)$$

with the rainfall intensity p (mm h^{-1}), the infiltration rate into the soil matrix i_{mat} (mm h^{-1}), and the macropore density n_{mac} (mm^{-2}).

We assessed the MDA for a given soil surface and macropore density with the following steps: (1) The surface topography (with a grid spacing of 1 cm) was either interpolated from the surveyed topography using Kriging with derived parameter for the exponential model (Table 2) or was generated randomly with a sequential Gaussian simulation program in GSLIB (Deutsch and Journel, 1992). The chosen grid spacing of 1 cm corresponds to the average opening size of an earthworm burrow at the soil surface. (2) The interpolated or generated topography was then overlaid with a rough surface representing the micro-topography. The micro-topography represented the roughness formed by vegetation, soil aggregates, or the activity of the earthworms, which often form a midden around the burrows by defecating soil particles and organic debris (Syers and Springett, 1983). As details about the micro-topography are generally unknown, a normally distributed random field with a standard deviation of 1 mm was used to reproduce this micro-topography. The flow direction of every cell of the ‘new surface’ was then calculated. The extent of depressions was determined iteratively starting at a local minimum (no flow cell). A depression was defined as the area where ponding could occur. Contiguous depressions were then merged and the topography underlying the depressions was raised to the height of the outlet of the depression.

(3) After a spatially random distribution of macropores for a defined macropore density was generated, the location of macropores was compared to the location of depressions. If a macropore was located within a depression, it was assumed to capture all water flowing into the depression. The flow accumulation for each cell was calculated according to the method of Holmgren (1984):

$$A_i = \frac{A(\tan \beta_i L_i)^h}{\sum_{i=1}^n (\tan \beta_i L_i)^h} \quad (4)$$

where n is the total number of downhill directions, A_i is the amount passed onto the i th downhill cell, A is the total up-slope area accumulated in the current cell,

481 $\tan \beta_i$ is the gradient and L_i is the contour length in the
 482 i th downhill cell and h is a weighting factor. If $h = 1$,
 483 the multiple-flow-direction algorithm by Quinn et al.
 484 (1991) was used. For $h > 100$, the single-flow-
 485 direction algorithm was implemented. We assumed
 486 dispersive flow at the soil surface, where h was set to
 487 two. After the flow accumulation for a macropore cell
 488 was calculated, the actual accumulated area was
 489 transferred to the macropore cell. This value was then
 490 the MDA of the macropore. The flow accumulation of
 491 this surface cell was then set to zero.

492 In order to reduce the influence of the boundary
 493 condition (no flow cell), only the MDA of the
 494 macropore cells located in the lower downslope half
 495 of the soil surface were considered (Weiler, 2001).
 496 The MDA of each macropore was normalized by the
 497 mean MDA; that is the surface area was multiplied by
 498 the macropore density. The normalized MDA of all
 499 macropores was then either summed up to calculate
 500 the total relative MDA or the cumulative probability
 501 distribution was derived. To account for different
 502 spatial distributions of the simulated macropores, 20
 503 realizations with different macropore distributions
 504 were derived for each of the four surface
 505 topographies.

507 2.5. Modelling of subsurface initiation

509 Our general approach for modelling subsurface
 510 initiation was similar to the surface initiation model.
 511 We considered a soil layer boundary with a sharp
 512 contrast in hydraulic conductivity where water excess
 513 would be generated and where, in this case, the water
 514 would flow under saturated conditions to macropore
 515 openings (themselves spatially randomly distributed
 516 and defined by the macropore density). In contrast to
 517 the surface initiation model, water flow is driven by
 518 the water table gradient, since the hydraulic head in
 519 the macropore is zero. A perched water table is built
 520 within a soil layer by the excess water, that is the
 521 difference between the recharge into the soil layer and
 522 the percolation from this layer. In addition to the
 523 surface initiation model, non-steady state conditions
 524 had to be considered as the amount of water stored in
 525 the porous media increases with time until the system
 526 reaches steady state conditions.

527 These prerequisites were accommodated by later-
 528 ally routing flow in a saturated layer above a low

529 permeable layer under Dupuit-Forchheimer assump-
 530 tions. The explicit grid-by-grid cell approach of
 531 Wigmosta and Lettenmaier (1999) was used for this
 532 routing. In contrast to most of the existing models
 533 defining the flow direction a priori by the surface
 534 topography, our approach recalculates the flow
 535 direction and outflow from each grid cell for each
 536 time step based on the local water table gradient.

537 The model was parameterized to account for a
 538 variety of factors that could change subsurface
 539 initiation. The parameters themselves were based on
 540 field measurements or observations. The reference
 541 simulation A (Table 4) was run with a macropore
 542 density (n_{mac}) of 250 m^{-2} , which is in the upper half
 543 of the observed range of macropore density (Table 1),
 544 but representing an average value of other studies.
 545 The spatially uniform saturated hydraulic conduc-
 546 tivity (k_s) is based on an average value estimated for
 547 the upper soil layers of the field sites (Table 1). The
 548 slope of the lower boundary was set to zero without
 549 topographic variations, conceptualized as a sharp,
 550 plane interface between two soil layers. For all
 551 simulations, the overall dimensions of the domain
 552 was set to 1 m by 1 m with a grid spacing of 1 cm.
 553 Each spatially random generated macropore was
 554 represented in the model by one grid cell with a
 555 hydraulic head of zero. The drainable porosity
 556 (effective porosity or specific yield) was set to 10%.
 557 Build up of the saturated zone in the modeled soil
 558 layer was driven by a recharge event of 3 h duration
 559 with a recharge intensity of 2 mm h^{-1} , thus represent-
 560 ing constant infiltration under unsaturated conditions
 561 ($2\text{--}5 \text{ mm h}^{-1}$). This layer of interest lies over a low
 562 permeable soil layer with an actual percolation rate
 563 between 0 and 3 mm h^{-1} . Three of four of the field
 564 sites in Switzerland exhibited such conditions. After
 565 the recharge event, the recession was simulated for
 566 another 5 h. Four additional simulations (B–E in
 567 Table 4) were run, where one of the following
 568 parameters was changed to explore possible influence
 569 factors: macropore density, spatial variability of
 570 saturated hydraulic conductivity, slope of the lower
 571 boundary, and roughness of the lower boundary.
 572 Hydraulic conductivity was varied applying a lognor-
 573 mally distributed spatially random conductivity field.
 574 The roughness of the lower boundary and thus the
 575 interface between the high and low permeable soil
 576 layer was described similarly to the generated surface

Table 4
Parameter settings for subsurface initiation model

Simulation	n_{mac} (m^{-2})	k_s (mm h^{-1})	Slope (%)	Lower boundary
A	250	6.0	0	Plane
B	100	6.0	0	Plane
C	250	6.0(± 1.3)	0	Plane
D	250	6.0	30	Plane
E	250	6.0	0	Rough ($\sigma = 10 \text{ mm}$, $a = 20 \text{ cm}$)

within the surface initiation model using an exponential variogram model.

In addition, we also tested the conditions under which a steady state assumption, and thus a simpler model, could be used to predict the MDA and thus the distribution of macropore flow initiation. For uniform hydraulic conductivity, steady state conditions, and a horizontal and plane boundary between the two soil layers, a macropore will drain the area that is closest to it in order to maximize gradient. This partition of the MDA can be described by the Voronoi diagram (Thiessen polygons) (see details in [Aurenhammer, 1991](#)). If a Poisson process is used to describe the spatially random distribution of macropores and the areal density of the generated random points, λ is equal to the macropore density, the size distribution of the MDA is equal the size distribution of random Voronoi segments that can be derived for one dimension ([Kiang, 1966](#)):

$$f(x) = \frac{c}{\Gamma(c)} (cx)^{c-1} e^{-cx} \quad (5)$$

where the Gamma distribution has the shape parameter $c = 2$ for the 1-D case and x is the normalized length. For the two dimensional case, the distribution becomes difficult to establish and no rigorously derived result has been published in the literature to date. However, simulations with randomly generated point patterns showed that for every areal density λ , c is equal to 4. ([Kiang, 1966](#)).

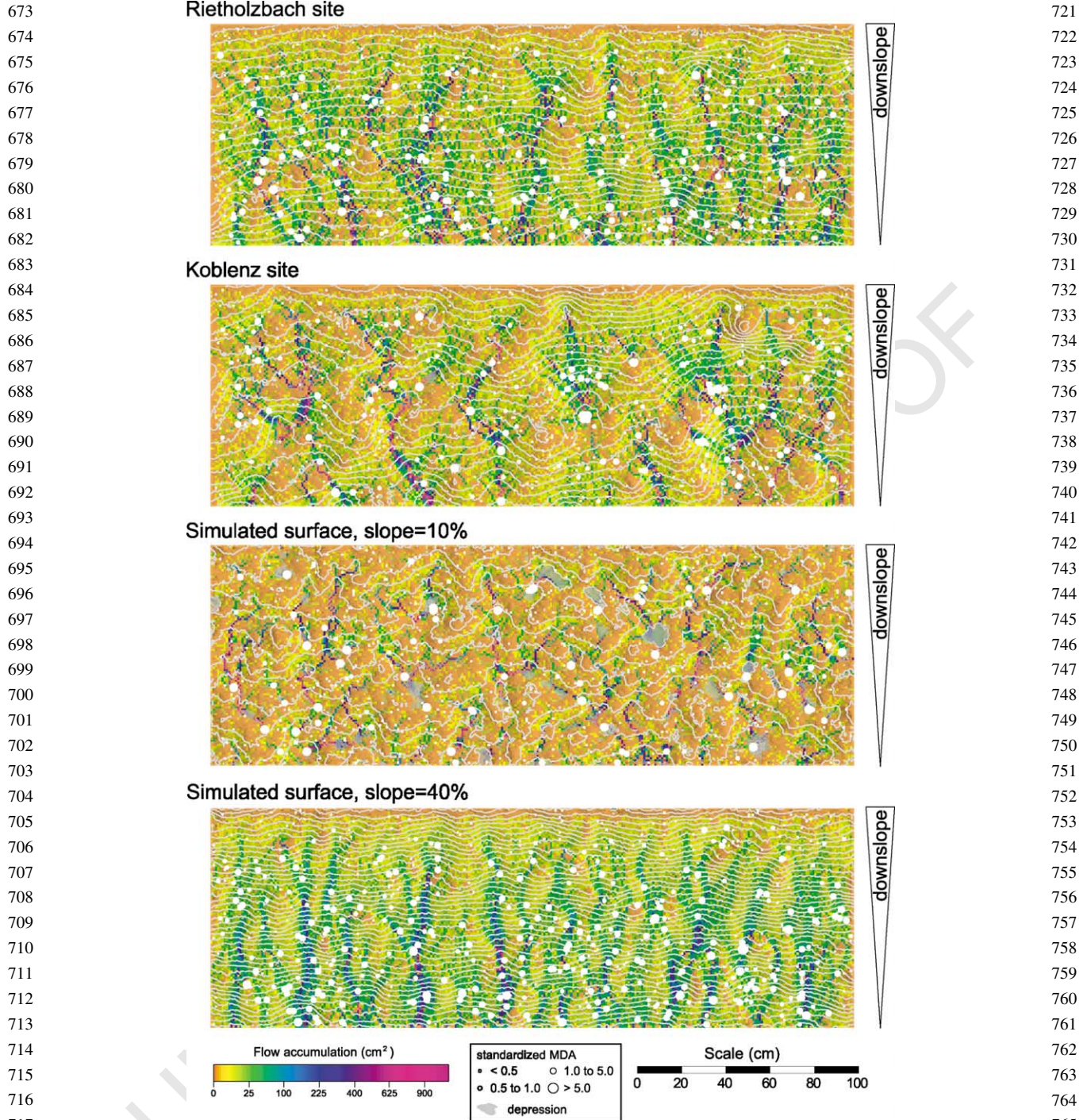
3. Results

The simulation results for surface initiation are presented for the measured surface topography and for

the simulated surface topography. The effect of the macropore density on total MDA and on the MDA probability distribution is assessed for the measured topography of the four sites. For the simulated surface topography the effects of the hillslope gradient on the MDA probability distribution are presented. The simulation results for subsurface initiation are described for the five different parameter sets in order to evaluate factors influencing the probability distribution of macropore initiation. Furthermore, the results of the dynamic simulations are compared with the steady state assumption that water in a saturated soil layer will flow to the nearest macropore. Finally, the distributions for surface and subsurface initiation are compared.

3.1. Surface initiation: macropore density and total MDA

The flow accumulation patterns at the soil surface with the MDA for each macropore for four selected realizations are shown in [Fig. 1](#) and will be used in the following to explain some findings. If the macropore density is low, the probability for water flowing on the soil surface to drain into a macropore is also low. Therefore, how strongly does the macropore density influence the MDA and thus the infiltration behaviour of the soil? For the four sites, the influence of the macropore density on the relative total MDA is illustrated in [Fig. 2](#). The error bars result from the 20 realizations for different spatial distributions of the simulated macropores. For comparison, the values of a plane surface with a gradient of 20% are shown. Especially for a density below 200 m^{-2} , the macropore density strongly influences the total relative MDA. Generally, the relationship was quite similar for the four sites. For macropore density between 100 and 250 m^{-2} , the Koblenz and Niederweningen sites in particular showed higher values. These two sites featured a higher absolute deviation of the surface from a fitted plane. This deviation was expressed as a higher surface roughness than the other two sites ([Table 2](#)). [Fig. 1](#) shows the flow accumulation pattern at the soil surface for the Rietholzbach and Koblenz site and illustrates, quantitatively, a possible explanation for the differences. For low roughness surface topography (Rietholzbach), a higher number of individual flow channels in hollows are observable



718 Fig. 1. Flow accumulation pattern at the soil surface for two surveyed sites (Rietholzbach and Koblenz) and for two simulated surfaces. Grey
719 lines are the contours with an elevation distance of 1 cm. The size of the macropore drainage area (MDA) for individual macropores is
720 superimposed by white dots.

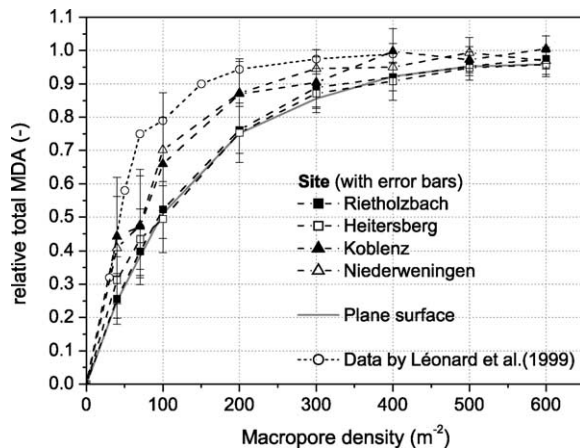


Fig. 2. Influence of macropore density on relative total macropore drainage area.

than for the high roughness surface topography (Koblenz). If the macropore density is low, the probability that macropores drain all flow channels is thus lower for the site with many flow channels. Therefore the total relative MDA is higher for the high roughness surface topography sites. The results for the low roughness surface topography are comparable to the MDA of a plane surface. Léonard et al. (2001) also derived a relation for macropore density and total MDA with a hydraulic model solving the 2-D St.Venant equation. Their values, which are similar to our results, are also shown in Fig. 2 and support the use of our approach to simulate the initiation process.

3.2. Surface initiation: macropore density and MDA probability distribution

Given our findings with macropore density and total MDA, we expected that the MDA probability distributions could show different behaviours. Fig. 3 shows the cumulative probability distribution of the MDA for different macropore densities at the four sites. Again, a difference between the low roughness surface topography sites (Rietholzbach and Heitersberg) and the high roughness surface topography sites (Koblenz and Niederweningen) are evident. For low roughness topography, the MDA was less than ~ 0.5 times the expected MDA for 50% of the macropores and the MDA was less than the expected MDA for 70% of the macropores. For high roughness topography, however, the MDA was less than ~ 0.5 times

the expected MDA for 70% of the macropores and the MDA was less than the expected MDA for 85% of the macropores. Furthermore, the MDA was more than 5 times larger than the expected MDA for only 2% of the macropores for the low roughness topography compared to over 4% for the high roughness topography. These differences can again be seen in Fig. 1. For low roughness topography, the channelling is low and thus only a few macropores receive a higher MDA. For high roughness topography, the channelling is high and thus macropores in the channels receive a high MDA. For all sites, the influence of the macropore density on the probability distribution is minor. There was a general trend that the cumulative probability distribution shifted to higher values if the normalized MDA was below two, but shifted to lower values if the normalized MDA was above two. This change could be related to the occurrence of high flow accumulation values. If the macropore density is low, the probability for high flow accumulation values is high. Thus, if a macropore is located within a hollow, its MDA is also high. However, as the channelling is more pronounced for a low macropore density, the macropores will have a lower MDA if their location is not in a hollow.

3.3. Surface initiation: hillslope gradient and MDA probability distribution

We used the results of the simulated surface topography to study the effects of the hillslope gradient. The simulated surface had similar spatial characteristics as the Rietholzbach and Koblenz sites with an underlying exponential model of scale $C = 1.35$ and range $a = 42$ cm. This simulated surface was then altered by changing the average deviation of the surface from a plane to 7 and 14 mm (similar to the observed values for the low and high roughness surface topography) and by introducing gradients from 0 to 40%. The results for the cumulative probability distributions are shown in Fig. 4. The distributions represent the average for the same four different macropore densities shown in Fig. 3. For the low roughness topography (Fig. 4(a)), the slope determined strongly the probability distribution. If the surface was flat or only slightly inclined (0–10%), 60% of the macropores drained an area smaller than 0.1 times the expected MDA, however,

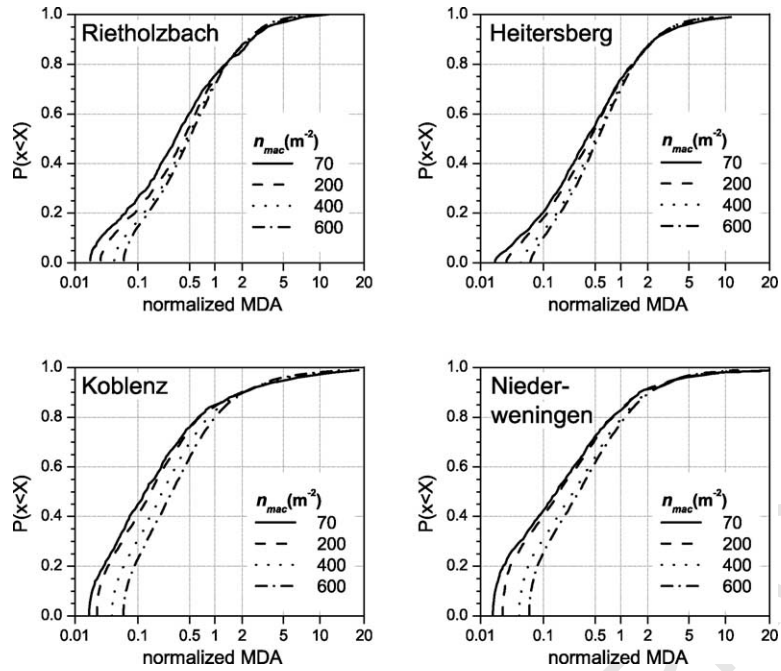


Fig. 3. Cumulative probability distributions for surface initiation of macropore drainage area for different macropore densities at the four sites (a) Rietholzbach, (b) Heitersberg, (c) Koblenz, and (d) Niederweningen.

around 2% of the macropores drained an area larger than 10 times the expected value. If the gradient was steep (40%), over 40% of the macropores drained an area between 0.5 and 2 times the expected value with only a few macropores that drained an area that was smaller than 0.1 times and larger than 5 times the expected MDA. The reason for this difference is visually apparent in Fig. 1. If the gradient is low (Fig. 1(c)), water flows into the nearest hollow, where the water accumulates. A macropore located in

the depressions receives a very high MDA, however, a macropore located on the ridge receives only a very low MDA. Because the total area with a low flow accumulation ($< 5 \text{ cm}^2$) is high, the probability is high that macropores are within this area. In contrast, the flow accumulation pattern looks different for the surface with a steep gradient (Fig. 1(d)). Because the roughness is low compared to the overall slope, water flows mainly in the direction of the slope and is channelled into the ‘valleys’. The area with

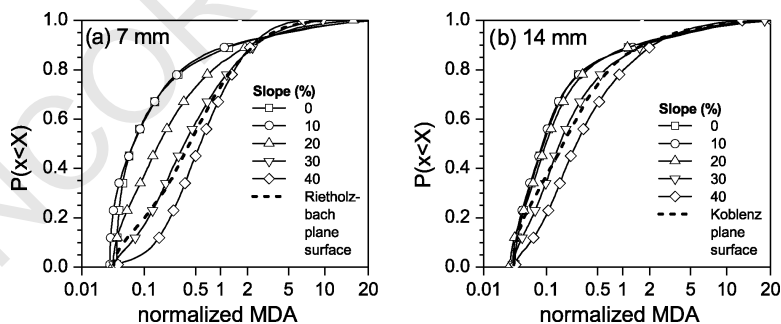


Fig. 4. Influence of the slope on the cumulative probability distribution for surface initiation of the macropore drainage area with (a) 7 mm average deviation and (b) 14 mm average deviation of the surface.

intermediate flow accumulation ($5\text{--}30\text{ cm}^2$) is high as water from higher elevation flows over a longer distance to lower elevation. Thus, the probability is high that macropores drain this intermediate flow accumulation. The probability for high MDA decreases as the channelling of water in the down-slope direction is more frequent. Comparing the results for the two different surface roughness conditions (Fig. 4(a) and (b)), the influence of the gradient is lower for the high surface topography. However, the same general pattern as in Fig. 4(a) is also valid for Fig. 4(b). The influence of the slope probably decreases because the water flows more directly into a depression or hollow, if the roughness of the soil surface is higher.

Fig. 4 also illustrates the distributions from the Rietholzbach and Koblenz sites for the measured topography with the results from the simulated surface topography. The average cumulative probability distribution for the Rietholzbach site matches the distribution for the simulated low roughness surface in Fig. 4(a) for a gradient of 30%. This value is higher than the measured gradient of 22% for the Rietholzbach site (Table 2), however, the general behaviour is similar for the measured and simulated surface topographies. The same results were found comparing the results of the site Koblenz with the simulated high roughness surface in Fig. 4(b). The distribution also matches best with the simulation results for a slope of 30%, despite a lower measured slope of only 16% for the site. In addition, the cumulative probability distribution calculated for a plane slope (Fig. 4) does not additionally influence the distribution. The resulting distribution is similar to a normal distribution with the median equal to the mean and a symmetrical shape. Consequently, the microtopography at the soil surface considerably changes the distribution of the MDA and thus the initiation of macropore flow.

3.4. Subsurface initiation: dynamic simulation and probability distribution of macropore initiation

Fig. 5 shows the flow from the saturated soil layer into the macropores for the five different simulations. The total flux is nearly similar for all simulations with a macropore density of 250 m^{-2} , and thus independent from the changing state parameters

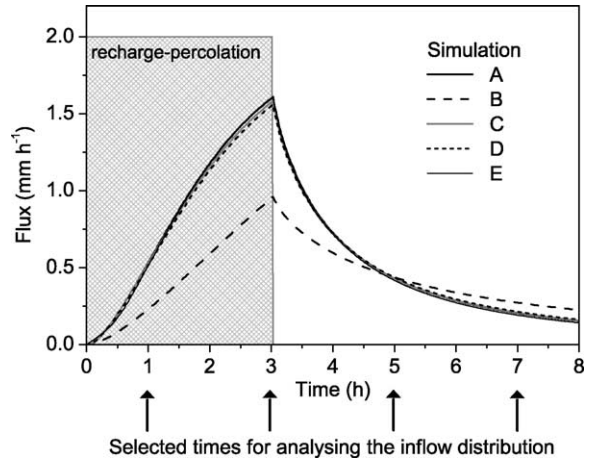


Fig. 5. Total flow from the saturated soil layer into the macropores during 5 different simulations and the selected times at which the probability distribution for subsurface initiation was analysed.

(Table 4). The flux for the simulation with the lower macropore density is lower due to lower average gradients. Fig. 5 also indicates the four selected times for calculating the initiation probability distribution: 1, 3, 5 and 7 h. The resulting normalized cumulative probability distribution for the reference simulation A and the simulation B is shown in Fig. 6. At 1 h, the distribution shows a low variance around the mean and a negative skewness, as the water table gradient towards the macropores is only fully developed in areas with a high macropore density. At 3 h (peak flux) the distribution is more symmetrical. At 5 and 7 h (during the recession after the input ended), the distributions are nearly similar with a positive skewness. If we compare these results to the steady-state assumption (Eq. 5), the distributions during recession match very closely the steady-state assumption. However, during the rising limb and peak, the distributions show a lower variance and different shape. Similar results can be observed for a lower macropore density (Fig. 6(b)). Here the distributions tend to develop slower towards the steady-state distribution, as the average spacing between the macropores is higher. The same results can also be observed for a lower hydraulic conductivity of the soil matrix or lower fluxes. Nevertheless, during recession the inflow distribution again matches closely the solution for steady-state conditions.

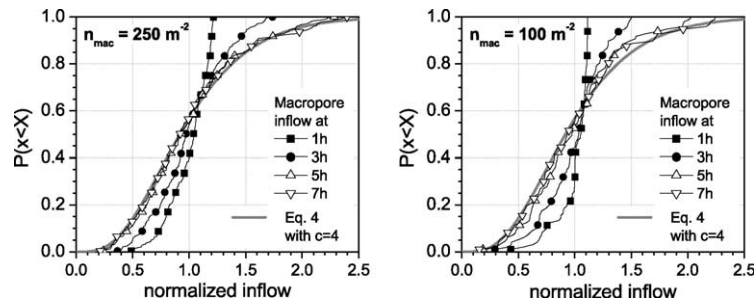


Fig. 6. Cumulative probability distributions of subsurface initiation flow at four selected times for (a) the reference simulation A with a macropore density of 250 m⁻² and (b) simulation B with a macropore density of 100 m⁻².

We then explored other possible influence factors on the probability distribution of macropore initiation. Fig. 7 shows the results for simulation C and E, which used a spatial variable k_s field and spatial variable lower boundary topography, respectively. The variable hydraulic conductivity did not influence the shape of the distributions. Compared to the reference simulation, the shape of the distribution at 1 h was even more similar to the steady state assumption. The results for the simulation with the rough interface between the high and low permeable soil layers show that this factor can influence slightly the shape of the distribution (Fig. 7(b)). For the simulation times of 1 and 3 h, the distributions are quite similar to the steady state assumption. However, during recession, the variance increased resulting in a flatter cumulative probability distribution. For simulation D (slope = 30%), the results are similar to simulation E and therefore not shown in detail. In summary, the derived distributions for subsurface initiation were variable due to the non-steady state behaviour of subsurface initiation. Nevertheless, the solution for

the steady state assumption was quite similar to most of the derived distributions for non-steady state.

3.5. MDA distribution for surface and subsurface initiation

Finally, the derived distributions of MDA for surface initiation at the four sites were compared with the distribution for subsurface initiation calculated for non-steady state condition with the explicit grid cell approach and for steady state condition according to Eq. 5 through their frequency distributions (Fig. 8). For surface initiation, the frequency distribution of the MDA showed an exponential behaviour with a high variance. The frequency distribution and therefore the distribution of macropore flow for surface initiation was influenced mainly by the surface topography. Only a few macropores, probably situated in depressions or hollows, contributed significantly to the water flow. The majority of macropores had a very low normalized MDA and thus received small amount of water. Other studies have also showed

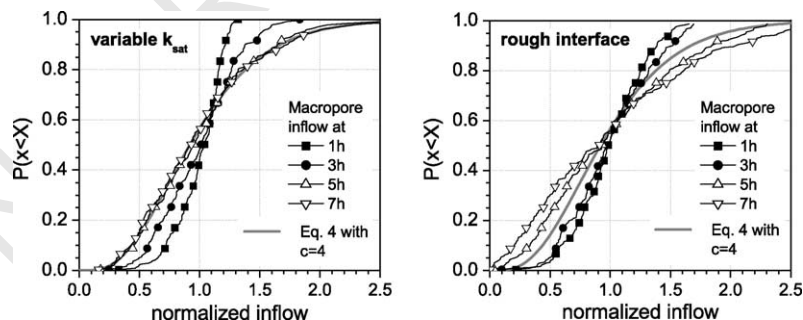


Fig. 7. Cumulative probability distributions of subsurface initiation flow at four selected times for (a) simulation C with a spatially variable saturated hydraulic conductivity field and (b) simulation E with a spatially variable lower boundary topography.

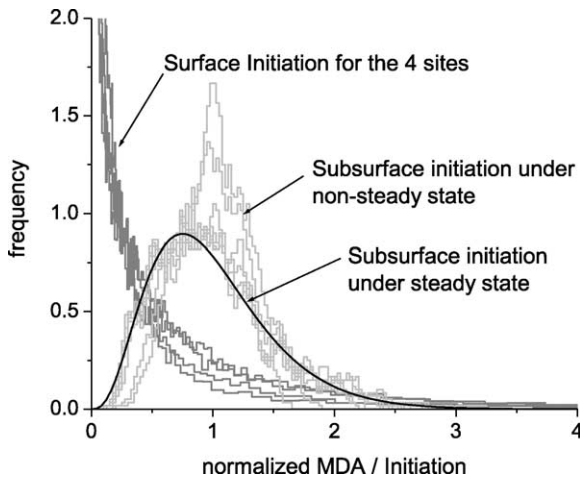


Fig. 8. Frequency distribution of the macropore drainage area for surface and subsurface initiation.

that the distribution of MDA initiated from the surface shows an exponential behaviour (Ela et al., 1992). Trojan and Linden (1992) measured a significant increase of macropore flow in macropores located in micro-depressions, since their MDA was larger than for macropores located on ridges. For subsurface initiation, in our study, the initiation probability distribution was more symmetrical and had a lower variance. The variance was especially small during recharge conditions. For the recession, the dynamic simulation resulted in similar probability distributions as for the steady-state assumption. We conceptualised that the subsurface initiation operates like a filter, equalizing the macropore flow compared to surface initiation, even if the properties of the soil layer are considered spatially variable. In general, macropore initiation provides a different supply of water into each macropore and thus causes a different water flux in each macropore.

4. Discussion

This study assessed the macropore flow initiation process at the surface and within the soil and the resulting flow rate distribution in vertical macropores formed by earthworm activity. We could show that macropore flow initiation results in a different supply

of water into each macropore depending on the surface topography, the macropore density, and the gradient of the soil surface. Now, we compare our solely simulation based results to various experimental findings and discuss the potentials to use our results to model water movement and solute transport in macroporous soils.

Combined sprinkling and dye tracer experiments at our four sites by Weiler and Naef (2002) provided one opportunity to observe indirectly the variation of flow rate in the macropores depending on the initiation process. Fig. 9 compares two classified dye patterns from horizontal soil sections. Tensiometer data and dye patterns from vertical sections confirmed that macropore flow was initiated at the soil surface (Fig. 9(a)) and within the topsoil (subsurface initiation) (Fig. 9(b)). The staining around macropores is proportional to the water flow from the macropores into the soil matrix. This interaction, however, depends on the actual flow rate within the macropores. Despite the fact that the total stained area around the macropores is different for the two sites, the variability of the stained area is larger for surface initiation. The dye pattern shows some macropores without staining and a few macropores where the staining is very large. For subsurface initiation, however, the stained areas around the macropores are quite similar. It should be noted that the hydraulic properties of the soil matrix were quite homogeneous for each horizontal soil sections. These differences in the dye patterns are reasonable, if the flow rate in the macropores and thus the interaction is variable depending on the initiation process.

A flow rate distribution within macropores resulting from macropore flow initiation has also been observed in several published laboratory experiments (Andreini and Steenhuis, 1990; Shipitalo et al., 1990; Edwards et al., 1992; Bowman et al., 1994; Quisenberry et al., 1994). In order to study the spatial and temporal variability of water and solute movement through intact soil blocks, it is necessary to interface the block with solution collection systems. Andreini and Steenhuis (1990) and Shipitalo et al. (1990) constructed the first grid lysimeter using a grid collector system. All experiments showed a high variability of water and solute flux among individual grid cells. Andreini and Steenhuis (1990) measured water

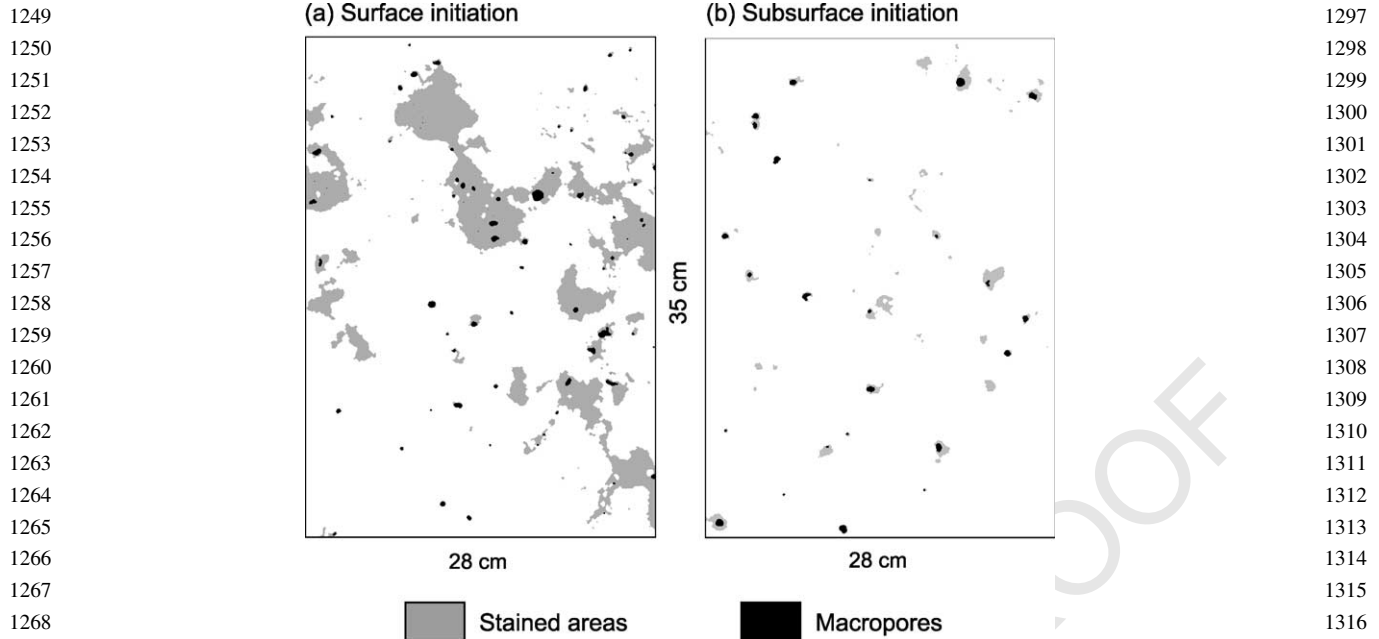


Fig. 9. Classified dye patterns of two horizontal soil sections, where macropore flow is initiated (a) at the soil surface (site Koblenz, $z = 50$ cm) and (b) within the topsoil (subsurface initiation) (site Heitersberg, $z = 40$ cm).

flow from only 30 to 40% of the total grid cells. Bowman et al. (1994) found that over 99% of the water flow was conducted through only about 26% of the basal area of the soil block, regardless of the application rate. They also conducted a bromide tracer experiments and found that approximately 85% of the water in the soil block was bypassed by the bromide. Quisenberry et al. (1994) also used different application rates ($5\text{--}31\text{ mm h}^{-1}$) and measured water flux and chloride concentration. Macropore flow was initiated at the grass covered soil surface. They found that 50% of the water and chloride appeared within 20% of the cross-sectional area. They always detected one grid cell in which the water flux was 3–30 times higher than the application rate. The water flux measurements of these published experiments correspond to our derived flow rate distribution for surface initiation. Edwards et al. (1992) measured percolate for a soil block with macropores formed by *Lumbricus terrestris* and found one grid cell comprised 30 to 60% of total percolate. Shipitalo and Edwards (1996), who also studied the influence of the initial

soil water content, found similar values. They concluded that the number of cells contributing to flow did significantly increase with increasing soil water content and argued that under dry condition macropore flow was initiated at the soil surface, and under wet conditions from a saturated zone near the soil surface.

We have not evaluated the impact of the initiation process for other types of macropores (root channels, cracks) and for other soil surface characteristics (forest, tillage). Furthermore, we have not considered temporally changing soil properties, like soil crust formation, soil erosion, soil management practice, or surface sealing. Also the dynamic of the whole macropore system due to earthworms closing holes and making new ones was not studied in more detail. Nevertheless, we hypothesize that the flow rates in all kind of macropores will not be the same as the area that drains into each macropore is always different. The actual MDA distribution for other types of macropores or soil surface characteristics can be different compared to the presented distributions, but the general approach to quantify their MDA should be

1345 the same. Thus we recommend that the approach
1346 outlined in this study be replicated for other types of
1347 macropores and other soil surface characteristics to
1348 receive a general description of flow rate distribution
1349 in macroporous soils. This flow rate distribution
1350 should then be considered for modelling infiltration in
1351 macroporous soils (Weiler, 2002).

1352
1353

1354 5. Conclusion

1355

1356 We confirm the importance of macropore flow
1357 initiation for infiltration and quantified the different
1358 amounts of water supplied to each macropore and thus
1359 the different water fluxes in each macropore. For
1360 surface initiation, the total MDA and therefore the
1361 proportion of overland flow that can drain into
1362 macropores is strongly influenced by the macropore
1363 density. A macropore density of 100 m^{-2} , which is a
1364 low value compared to field observations (Weiler and
1365 Naef, 2002), is sufficient to capture between 50 and
1366 80% of the overland flow. The probability distribution
1367 of the MDA and therefore the distribution of
1368 macropore flow from surface initiation is influenced
1369 mainly by the surface topography. We found that only
1370 a few macropores contribute significantly to the water
1371 flow, especially for a irregular and rough surface
1372 topography and for a low soil surface gradient.
1373 However, these differences are minor compared to
1374 the derived distribution for subsurface initiation or
1375 compared to the common assumption of the same flow
1376 rate in each macropore. The probability distribution of
1377 macropore flow for subsurface initiation is more
1378 symmetrical and has a lower variance than that for
1379 surface initiation. This difference changes slightly
1380 depending on the developed gradient of the water
1381 table in the saturated soil layer and the heterogeneities
1382 in the soil. Independent from these various and related
1383 factors, the probability distribution for subsurface
1384 initiation is distinctly different from the distribution
1385 for surface initiation.

1386 The actual macropore flow distribution probably
1387 differs somewhat from the simulated distributions, as
1388 macropore flow initiation is a dynamic process and
1389 soil properties are often more heterogeneous than the
1390 simulations can reproduce. Flow rates in macropores
1391 are certainly not identical—the two studied cases of
1392 surface and subsurface initiation approximate the

envelope of the flow rate distribution in continuous
earthworm macropores.

1393
1394

Acknowledgements

This work was funded by the Swiss Federal
Institute of Technology in Zürich within the project
'Investigation of the water exchange mechanisms
between preferential flow paths and the soil matrix'.
We thank Jeff McDonnell, Kerstin Stahl, and Brian
McGlynn for improving the final manuscript.

1395
1396
1397
1398
1399
1400
1401
1402
1403
1404

References

- 1405
1406
1407
1408
1409
1410
1411
1412
1413
1414
1415
1416
1417
1418
1419
1420
1421
1422
1423
1424
1425
1426
1427
1428
1429
1430
1431
1432
1433
1434
1435
1436
1437
1438
1439
1440
- Andreini, M.S., Steenhuis, T.S., 1990. Preferential paths of flow under conventional and conservation tillage. *Geoderma* 46, 85–102.
- Aurenhammer, F., 1991. Voronoi diagrams—a survey of a fundamental geometric data structure. *ACM Computing Surveys* 23 (3), 345–405.
- Beven, K., Germann, P., 1982. Macropores and water flow in soils. *Water Resour. Res.* 18 (5), 1311–1325.
- Bouma, J., Belmans, C.F.M., Dekker, L.W., 1982. Water infiltration and redistribution in a silt loam subsoil with vertical worm channels. *Soil Sci. Soc. Am. J.* 46, 917–921.
- Bowman, B.T., Brunke, R.R., Reynolds, W.D., Wall, G.J., 1994. Rainfall simulator-grid lysimeter system for solute transport studies using large, intact soil blocks. *J. Environ. Qual.* 23, 815–822.
- Brimicombe, A.J., Tsui, P.H.Y., 2000. A variable resolution, geocomputational approach to the analysis of point patterns. *Hydrological Processes* 14, 2143–2155.
- Buttle, J.M., House, D.A., 1997. Spatial variability of saturated hydraulic conductivity in shallow macroporous soils in a forested basin. *J. Hydrol.* 203, 127–142.
- Deutsch, C.V., Journel, A.G., 1992. *GSLIB—Geostatistical Software Library and Users Guide*, Oxford University Press, New York.
- Diggle, P.J., 1983. *Statistical Analysis of Spatial Point Patterns*, Academic Press, London.
- Droogers, P., Stein, A., Bouma, J., de Boer, G., 1998. Parameters for describing soil macroporosity derived from staining patterns. *Geoderma* 83, 293–308.
- Edwards, W.M., Shipitalo, M.J., Dick, W.A., Owens, L.B., 1992. Rainfall intensity affects transport of water and chemicals through macropores in no-till soil. *Soil Sci. Soc. Am. J.* 56, 52–58.
- Ehlers, W., 1975. Observation on earthworm channels and infiltration on tilled and untilled loess soil. *Soil Sci.* 119 (3), 242–249.
- Ela, S.D., Gupta, S.C., Rawls, W.J., 1992. Macropore and surface seal interactions affecting water infiltration into soils. *Soil Sci. Soc. Am. J.* 56, 714–721.
- Faeh, A.O., Scherrer, S., Naef, F., 1997. A combined field and numerical approach to investigate flow processes in natural macroporous soils under extreme precipitation. *Hydrol. Earth Syst. Sci.* 4, 787–800.

- 1441 Flüßler, H., Durner, W., Flury, M., 1996. Lateral solute mixing
1442 processes-A key for understanding field-scale transport of water
1443 and solutes. *Geoderma* 70, 165–183. 1489
- 1444 Food and Agricultural Organization, 1974. FAO-UNESCO Soil
1445 Map of the World, 1:5000000, vol. I., Legend, Unesco, Paris. 1490
- 1446 Holmgren, P., 1984. Multiple flow direction algorithms for runoff
1447 modelling in grid based elevation models: an empirical
1448 evaluation. *Hydrol. Processes* 8, 327–334. 1491
- 1449 Huang, C.-H., 1998. Quantification of soil microtopography and
1450 surface roughness. In: Baveye, P., Parlange, J.-Y., Stewart, B.A.
1451 (Eds.), *Fractals in soil science*, CRC Press, Boca Raton. 1492
- 1452 Kiang, T., 1966. Random fragmentation in two and three
1453 dimensions. *Zeitschrift für Astrophysik* 64, 433–439. 1493
- 1454 Langmaack, M., Schrader, S., Rapp-Bernhardt, U., Kotzke, K.,
1455 1999. Quantitative analysis of earthworm burrow systems with
1456 respect to biological soil-structure regeneration after soil
1457 compaction. *Biol. Fertil. Soils* 28, 219–229. 1494
- 1458 Larson, M., 1999. Quantifying macropore flow effects on nitrate and
1459 pesticide leaching in a structured clay soil, *Field Experiments
1460 and Modelling with the MACRO and SOILN Models*, Swedish
1461 University of Agricultural Science. 1495
- 1462 Léonard, J., Esteves, M., Perrier, E., de Marsily, G., 1999. A
1463 spatialized overland flow approach for the modelling of large
1464 macropores influence on water infiltration. *International Work-
1465 shop of EurAgEng's Field of Interest on Soil and Water,
1466 Leuven*, 313–322. 1496
- 1467 Léonard, J., Perrier, E., de Marsily, G., 2001. A model for simulating
1468 the influence of a spatial distribution of large circular macropores
1469 on surface runoff. *Water Resour. Res.* 37 (12), 3217–3225. 1497
- 1470 Li, Y., Ghodrati, M., 1997. Preferential transport of solute through
1471 soil columns containing constructed macropores. *Soil Sci. Soc.
1472 Am. J.* 61, 1308–1317. 1498
- 1473 Munyankusi, E., Gupta, S.C., Moncrief, J.F., Berry, E.C., 1994.
1474 Earthworm macropores and preferential transport in a long-term
1475 manure applied typic Hapludalf. *J. Environ. Qual.* 23, 773–784. 1499
- 1476 Phillips, R.E., Quisenberry, V.L., Zeleznik, J.M., Dunn, G.H., 1989.
1477 Mechanism of water entry into simulated macropores. *Soil Sci.
1478 Soc. Am. J.* 53 (6), 1629–1635. 1500
- 1479 Quinn, P.F., Beven, K.J., Chevallier, P., Planchon, O., 1991. The
1480 prediction of hillslope flow paths for distributed hydrological
1481 modelling using digital terrain models. *Hydrol. Processes* 5,
1482 59–79. 1501
- 1483 Quisenberry, V.L., Phillips, R.E., Zelenzik, J.M., 1994. Spatial
1484 distribution of water and chloride macropore flow in a well-
1485 structured soil. *Soil Sci. Soc. Am. J.* 58, 1294–1300. 1502
- 1486 Schaap, M.G., Leij, F.J., 2000. Improved prediction of unsaturated
1487 hydraulic conductivity with the Mualem-van Genuchten model.
1488 *Soil Sci. Soc. Am. J.* 64, 843–851. 1503
- 1489 Shipitalo, M.J., Edwards, W.M., 1996. Effects of initial water
1490 content on macropore-matrix flow and transport of surface-
1491 applied chemicals. *J. Environ. Qual.* 25 (4), 662–670. 1504
- 1492 Shipitalo, M.J., Edwards, W.M., Dick, W.A., Owens, L.B., 1990.
1493 Initial storm effects on macropore transport of surface-applied
1494 chemicals in no-till soil. *Soil Sci. Soc. Am. J.* 54 (6),
1495 1530–1536. 1505
- 1496 Shipitalo, M.J., Gibbs, F., 2000. Potential of earthworm burrows to
1497 transmit injected animal wastes to tile drain. *Soil Sci. Soc. Am.
1498 J.* 64, 2103–2109. 1506
- 1499 Smettem, K.R.J., Collis-George, N., 1985. Statistical characteriz-
1500 ation of soil biopores using a soil peel method. *Geoderma* 36,
1501 27–36. 1507
- 1502 Soil Survey Staff, 1951. *Soil survey manual*, US Department of
1503 Agriculture Handbook, 18. 1508
- 1504 Stein, A. (Ed.), 1999. *Spatial Statistics for Remote Sensing*, Kluwer,
1505 Dordrecht. 1509
- 1506 Syers, J.K., Springett, J.A., 1983. Earthworm ecology in grassland
1507 soils. In: Satchell, J.E., (Ed.), *Earthworm Ecology*, Chapman
1508 and Hall, London. 1510
- 1509 Trojan, M.D., Linden, D.R., 1992. Microrelief and rainfall effects
1510 on water and solute movement in earthworm burrows. *Soil Sci.
1511 Soc. Am. J.* 56, 727–733. 1511
- 1512 Trojan, M.D., Linden, D.R., 1998. Macroporosity and hydraulic
1513 properties of earthworm-affected soils as influenced by tillage
1514 and residue management. *Soil Sci. Soc. Am. J.* 62 (6),
1515 1687–1692. 1512
- 1516 Wang, D., Norman, J.M., Lowery, B., McSweeney, K., 1994.
1517 Nondestructive determination of hydrogeometrical character-
1518 istics of soil macropores. *Soil Sci. Soc. Am. J.* 58 (2), 294–303. 1513
- 1519 Weiler, M., 2001. Mechanisms controlling macropore flow during
1520 infiltration-dye tracer experiments and simulations. *Diss. ETHZ
1521 No. 14237*, Zürich, Switzerland. <http://e-collection.ethbib.ethz.ch/cgi-bin/show.pl?type=diss&nr=14237>. 1514
- 1522 Weiler, M., 2002. A new approach to describe infiltration into soils
1523 containing macropores. *Water Resour. Res.* in review. 1515
- 1524 Weiler, M., Naef, F., 2002. An experimental tracer study of the role
1525 of macropores in infiltration in grassland soils. *Hydrol.
1526 Processes* in press. 1517
- 1527 Weiler, M., Naef, F., Leibundgut, C., 1998. Study of runoff
1528 generation on hillslopes using tracer experiments and physically
1529 based numerical model. *IAHS Publications* 248, 353–360. 1518
- 1530 Wigmosta, M.S., Lettenmaier, D.P., 1999. A comparison of
1531 simplified methods for routing topographically driven subsur-
1532 face flow. *Water Resour. Res.* 35, 255–264. 1519
- 1533 Zehe, E., Flüßler, H., 2001. Slope scale variation of flow patterns in
1534 soil profiles. *J. Hydrol.* 247, 116–132. 1520